PULLING TRACTOR RING GEAR ANALYSIS

Mee631 Group 5

Group Members+Percent of Work

Kyle Jackson 25%
Adnan Rasheed 25%
Mujahid Mohammed 25%
Abdul Kaleem Mohammad 25%

Contents

Introduction 4
Background 4
Problem Statement 4
Project Goal 5
Analysis Type 6
Literary Search 6
Geometry and Force Calculations 6
Gear Geometry 6
Force Calculations 8
Engine Torque 8
Gear Forces 8
Analytical gear stress 10
ANSYS APDL Analysis 11
General Mesh 11
Static Analysis 11
Static Analysis Boundary Conditions 11
Static Analysis Full Model Mesh 12
Sub Model Mesh 14
Static Convergence Study 15
Static Analysis Results 15
Contact Analysis 18
Contact Analysis Mesh 18
Contact Analysis Boundary Conditions 19
Contact Analysis Convergence Study 20
Contact Analysis Results 21
Result Conclusion 24
Challenges Overcome 24
Future Work 25
Works Citied 26
APPENDIX 28

Ring Gear Drawing 28
Pinion Gear Drawing 29
MATLAB FORCE CALCUATION CODE 30
Static Convergence Mesh 31

Figure 1: Types of Bevel Gears 4
Figure 2: Modified Cub Cadet Tractor 4
Figure 3: Ring Gear Teeth failure 5
Figure 4: Ring Gear and Differential Failure 5
Figure 5: Ring Gear 3D Model 7
Figure 6: Pinion Gear 3D Model 7
Figure 7: Ring and Pinion Gear Assembly 8
Figure 8: Cub Cadet Transaxle. [2] 9
Figure 9: Gear Force Components [Shigley's p.709 Figure 13-35] 10
Figure 10: Soild187 Element 11
Figure 11: Ring Gear Displacement Constraints 12
Figure 12: Ring Gear Tooth Pressure 12
Figure 13: Full Ring Gear Model Mesh 13
Figure 14: Zoomed in Teeth Mesh 13
Figure 15: Course Sub Model Mesh Element Size .2 in 14
Figure 16: Refined Sub Model Mesh .05 in Element Size 14
Figure 17: Static Analysis Convergence Study 15
Figure 18: Full Model Deformation 15
Figure 19: Sub Model Deformation 16
Figure 20: Full Model Von-Mises Stress 17
Figure 21: Sub Model Von-Mises Stress 17
Figure 22: Full Ring and Pinion Mesh Element Size .09 in 18
Figure 23: Contact Elements 19
Figure 24: Contact Boundary Conditions 20
Figure 25: Contact Stress Convergence 20
Figure 26: Contact Pressure Convergence 21
Figure 27: Contact Analysis Von-Mises 22
Figure 28: Ring Gear Tooth Chipping 23
Figure 29: Contact Pressure Plot 23
Figure 30: Poor Mesh Transition Areas. 24

Introduction

Background

Bevel gear pairs are common in many mechanical systems. Many modern day vehicles use a type of bevel gear system in their drive axles. With the ability for bevel gears to allow for a change in shaft orientation other than the parallel change that spur type gears allow. The bevel gears also have the ability to be created in different tooth profiles. These profiles are Straight, Spiral, and Hypoid. An example of each of these gears is shown below in Figure 1.

Figure 1: Types of Bevel Gears

The straight bevel gears have a conical pitch surface with teeth that are straight and tapering towards the gear center. Spiral gears on the other hand have angled curve teeth that also taper toward the center. The advantage to the spiral gear is smoother, more gradual tooth contact. The final hypoid type has gear teeth much like the spiral gear but the teeth are hyperbolic. The last type of gears is most commonly found in automotive rear ends. With the use of any gear system the loads, speeds, and type of loading play a major part in the stress and wear on the components. In this project we are looking into the stress and deflection of a straight bevel gear pair from a Cud Cadet garden tractor.

Problem Statement

The Cub Cadet garden tractor ring and pinion gear that is being analyzed was being used in a modified tractor that saw severe duty use in tractor pulling. This tractor had the original engine replaced with a modified engine that is capable out producing 30 horsepower at 4000 RPM. The tractor is shown below in Figure 2.

Figure 2: Modified Cub Cadet Tractor

This is more than double the original engine specifications the tractor had. With these modifications breakages of the ring and pinion sets have occurred. These failures have occurred in two major ways. The first of which has been an individual tooth have either cracked or sheared off the ring and pinion gear. This type of failure can be seen below in Figure 3.

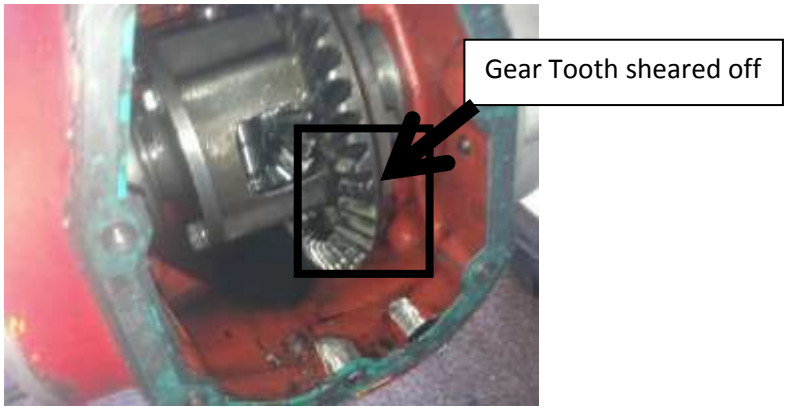

Figure 3: Ring Gear Teeth failure

The second major type of failure that has occurred is the ring and pinion gear's mesh separating and causing large deformations in the ring gear or differential. This deformation leads to the gear teeth failing or the differential shearing. Once this differential fails more gear teeth will soon follow. This type of failure can be seen in Figure 4.

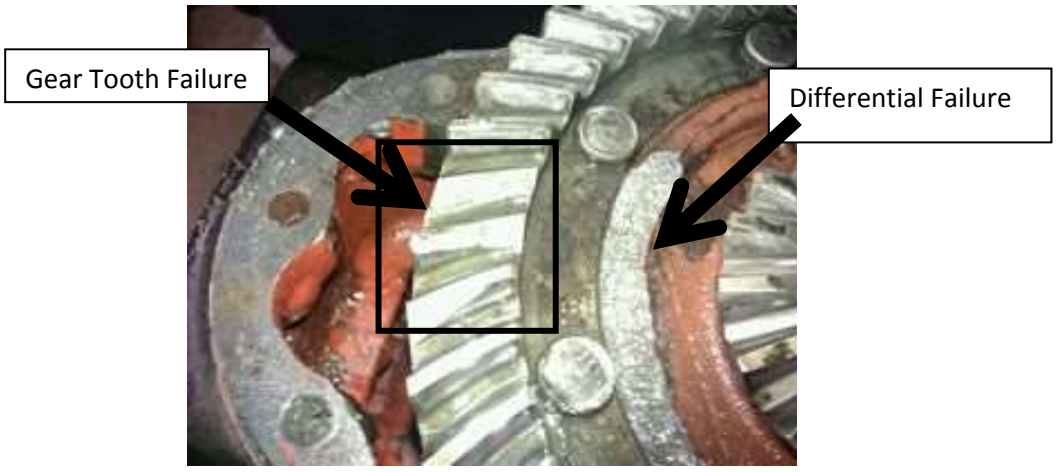

Figure 4: Ring Gear and Differential Failure

With these failures the tractor must be torn down for service and repair. This repair can range from 3-5 hours for a ring and pinion gear and cost between $60 and $100, if the differential is also damaged like in Figure 4, the repair time increases by one hour and the cost also rises by $100-$200. When these parts fail the tractor is unable to further compete in the pull, due to no longer being able to move or unable to move under heavy load.

Project Goal

The goal of this analysis is to study the possible location and causes of failures. The two causes of failure that will be looked at are those due to tooth stress and gear deformation. The tooth stress failure would cause the teeth to shear off, much like in Figure 3. Whereas the gear deformation would cause the teeth to leave mesh, allowing the contact ratio to fall below one, which would shear or deform the teeth leading to a failure like in Figure 4.

Analysis Type

The analysis will be conducted by performing a static structural analysis on the ring gear and a contact analysis between both of the gears. With these two results we will be able to determine if the gear teeth are failing on the ring gear under static loading or if the gears are failing under dynamic loading.

Literary Search

Bending Stress Analysis of Bevel Gears Ratnadeepsinh M. Jadeja, Dipeshkumar M. Chauhan, Jignesh D. Lakhani.

The research modeled single gear teeth and applied the pressure to a small area created on the gear tooth surface. This allowed for a closer to actual line pressure the mating gear teeth would have. This analysis would be able to be conducted using only the ring gear model, which would further reduce the number of need nodes.

Friction Tooth Contact Analysis along line of action of a spur Gear using Finite Element Method Santosh Patil, Saravanan Karuppannan, Ivana Atanasovska, Azmi A Wahab.

The paper looks at modeling the line of action of gear teeth entering and exiting mesh. The paper looks at spur gears but, their method of modeling sections of the gear with a smaller number of teeth allows for a finer mesh.

Finite Element Analysis of High Contact Ratio Gear M. Rameshkumar, G. Venkatesan, P. Sivakumar

The paper looks into creating two meshed gears. The gears base circle is completely modeled while only small sections of mating teeth are added to the model. This paper also conducts a contact analysis on the gear teeth that are modeled.

Bevel Gear Tooth Bending Stress Evaluation Using Finite Element Analysis Emre Turkoz, Can Ozcan

The paper models helical gears and conducts a study on the bending stress of the gear. The paper talks about applying section of beam joint elements to add in rotational degrees of freedom for the system, since the tetrahedron elements do not support it.

Geometry and Force Calculations

Gear Geometry

The gear models were created form actual parts removed from a Cub Cadet pulling tractor. The gears consisted of a straight cut ring gear and matching straight pinion gear. The SolidWorks models of the gears are shown below in Figure 5and Figure 6.

Figure 5: Ring Gear 3D Model

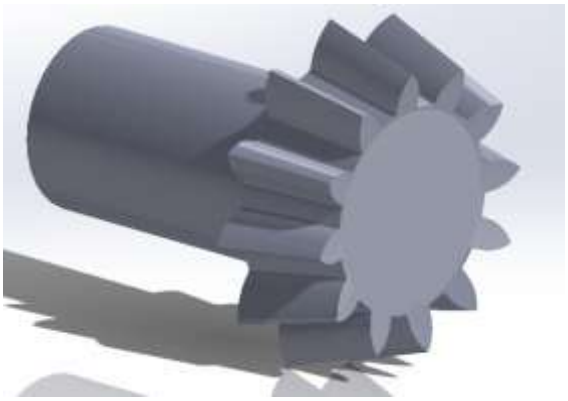

Figure 6: Pinion Gear 3D Model

Both Gear models were created with the use of the bevel gear toolbox in SolidWorks. The dimensions needed to create the gears in the toolbox are show in table 1 for both the ring and pinion gear.

Table 1: Gear Dimensions

Gear name	Ring Gear	Pinion Gear
Number of Teeth	46	12
Diametric Pitch	6	6
Face width	.75	.75
Bore diameter	4.5	NA
Shaft diameter	NA	1.25
Mounting Distance	.175	2.125
Material	Hardened Steel	Hardened Steel

Also for use in this project an assembly of the gears was created for use in the contact analysis. This assembly is shown below in Figure 7. The 2d drawings for the gears are included in the appendix.

Figure 7: Ring and Pinion Gear Assembly

Force Calculations

To apply the proper loading to the gears in the analysis the gear forces must be calculated from the known geometry and engine specifications. These values will also be needed for calculating the analytical stress values to compare the ANSYS results to.

Engine Torque

The engine torque output torque can be found from the engine specifications known. The engine operates with a maximum horse power of 30 H.P. at a speed of 4000 RPM. With these values the engine torque can be found using Equation 1.

Equation 1

$$T_{eng} = \frac{HP * 33000}{2 * \pi * rpm}$$

Where HP is engine horsepower and rpm is engine speed.

The engine is found to produce a maximum torque of 39.39 lbs*ft. This torque is directly applied to the input shaft of the transaxle by a steel driveshaft and friction clutch. The engine transfers the full amount of torque to the transaxle when the clutch is fully released.

Gear Forces

The driveshaft of the tractor is attached to the reduction hosing input shaft. This housing has an internal gear ratio of 7/1. this then drives the top shaft in the shift-able portion of the transaxle. The final gear ratio for the top shaft of the transaxle to the pinion gear shaft is a 1.48-1 ratio. This configuration can be seen below in Figure 8: Cub Cadet Transaxle. [2], where the path taken through the gear box is shown by the black bold line.

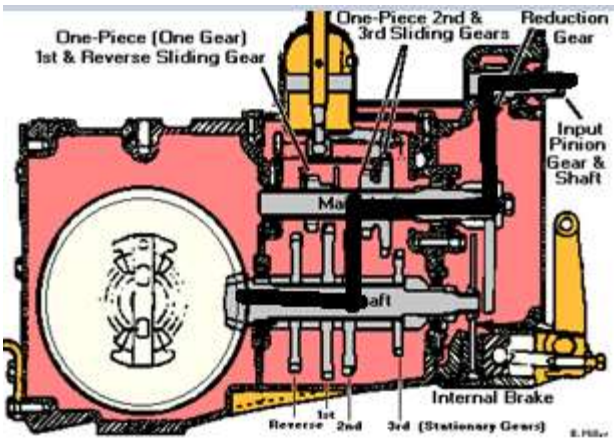

Figure 8: Cub Cadet Transaxle. [2]

This brings the final drive ratio from the engine shaft to the 10.33-1. The torque on the pinion gear shaft can be calculated using Equation 2.

Equation 2

$$T_{pshaft} = T_{eng} * ratio_{final}$$

Where: T_{eng} is the engine torque, $ratio_{final}$ is the final drive ratio of the transaxle, and T_{pshaft} is the torque applied to the pinion shaft. The final calculation was to find the force onto the gear tooth parallel to the pressure angle. This force was found via Equation 3.

Equation 3 [2]

$$W = ShaftTorque/(ravg * \cos(Delta))$$

Where shaft torque is the torque on the gears input shaft in ft*lbs, ravg is the gear pitch radius in feet, and delta is the pressure angle of the gear in degrees. With the use of the gear geometry and the previously calculated torque the force was found to be 5631.81 lbs. This force can be seen as W in XXXX

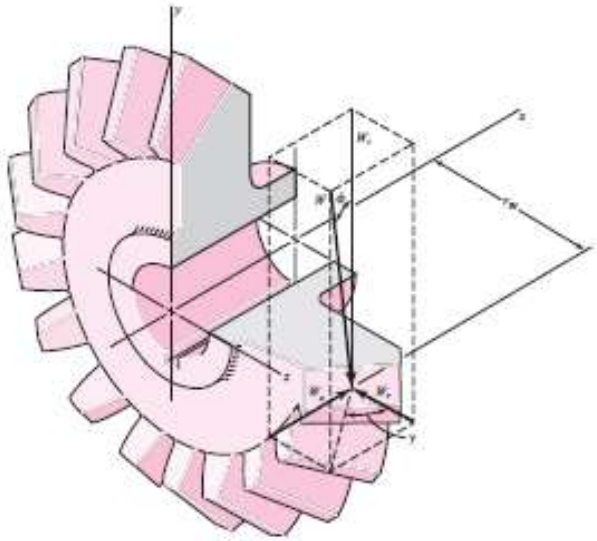

Figure 9: Gear Force Components [Shigley's p.709 Figure 13-35]

Analytical gear stress

The gear stress for both the static and contact analysis was calculated to allow for comparison of the APDL results to an analytical value. The values are based on the type of loading, mounting characteristics, and geometry factors. The calculation for the single ring gear static stress was found using the AGMA Stress equation (Equation 4) and the AGMA Bending Stress Equation (XXXXX)

Equation 4 (Shigley's pg.787 equation 15-1)

$$\sigma_c = C_p * \left(\frac{W}{F * pd * I} * K_o * K_v * K_m * C_s * CX_c \right)$$

Where: C_p is the elastic coefficient, W is gear force, F is face width, pd is diametric pitch, I is geometry factor for pitting resistance, K_o is over load factor, K_v is dynamic factor, K_m is the load distribution factor, C_s is size factor for pitting resistance, C_{xc} is crowning factor for pitting resistance.

Equation 5 (Shigley's pg.791 equation 15-2)

$$ST = \left(\frac{W}{F} \right) * pd * K_0 * K_v * (K_s * K_m)/J$$

Where: W is gear force, F is face width, pd is diametric pitch, K_o is overload factor, K_v is dynamic factor, K_s is size factor for bending, K_m is load distribution factor, and J is geometry factor for bending strength.

These constant values are shown below in Table 2, the graphs needed to calculate the values are included in the appendix.

Table 2: Gear Stress Parameters

C_p	.29	K_v	1.4
W	5631.81 lbs	K_m	1.1002
F	.75 in	C_s	.5312
Pd	6	C_{xc}	2
I	.0075	K_s	.5231
K_o	1.25	J	.165

The analytical values there were calculated from these equations are σ_c= 49,497 psi, and ST=234,920 psi. These values will be used later for comparison with the FEM results.

ANSYS APDL Analysis

General Mesh

The 3d models were converted to .IGES files for importing into ANSYS APDL. This file type allows for the 3d model to be used as either a surface or solid, the models for this analysis were imported as solids. The element type that was used for this model was that of Solid187. This element is a 10 node tetrahedral element used to mesh volumes. This element is good for meshing complex surfaces that brick elements cannot mesh. The element is shown below in Figure 10.

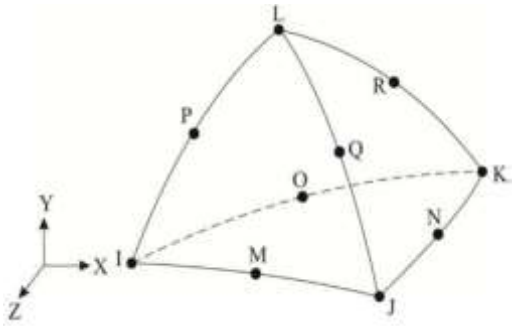

Figure 10: Soild187 Element

Static Analysis

The static analysis was conducted to simulate the load onto one ring gear tooth when the tractor has not started moving. This analysis was conducted to see if the ring gear teeth were failing under static loading when only one set of teeth were in mesh.

Static Analysis Boundary Conditions

The boundary conditions applied to the ring gear for the static analysis were chosen such that the ring gear would remain fixed along the same area as when it is mounted inside the tractor. To replicate this ring gear was fixed along a portion of the rear surface of the gear in all directions, this can be seen below in Figure 11.

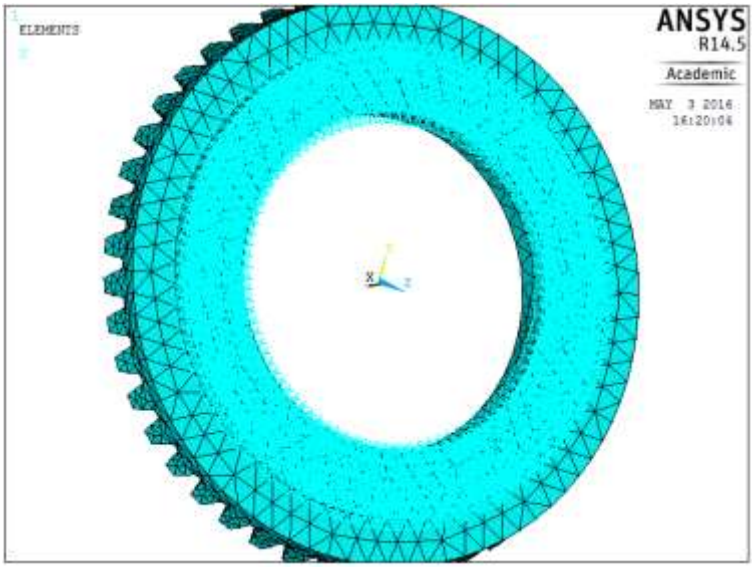

Figure 11: Ring Gear Displacement Constraints

The ring gear also had a pressure applied to the face of a single tooth. This can be seen below in Figure 12.

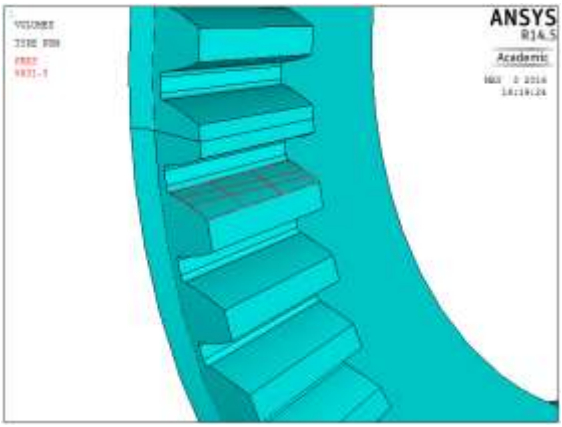

Figure 12: Ring Gear Tooth Pressure

Static Analysis Full Model Mesh

The model must be meshed with a fine enough mesh that the results converge to value. This mesh, shown below in Figure 13, was created using a free mesh with an element size of .5 in. this mesh can be seen to be very course.

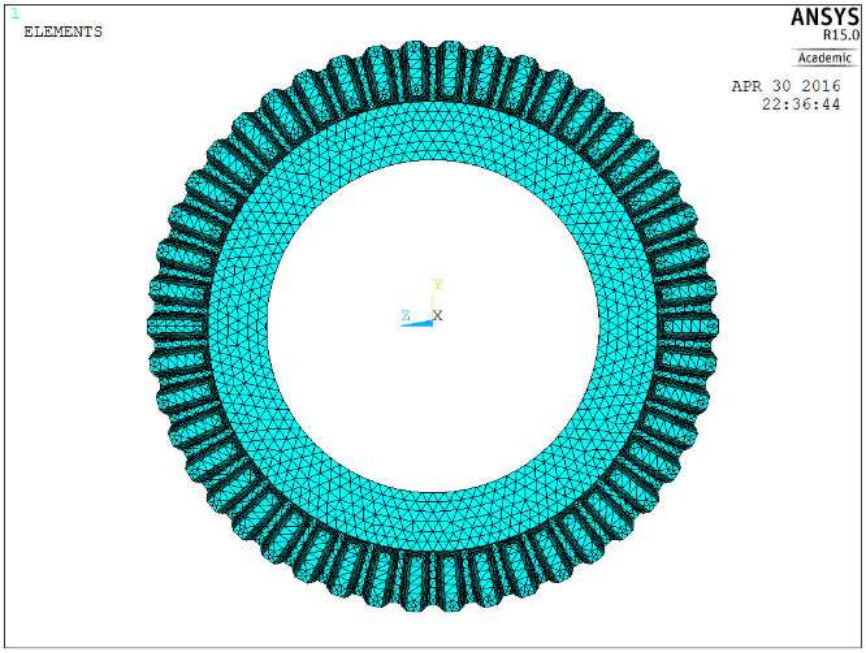

Figure 13: Full Ring Gear Model Mesh

The areas around the teeth also have poor transitions and limited number of elements as can be seen in Figure 14.

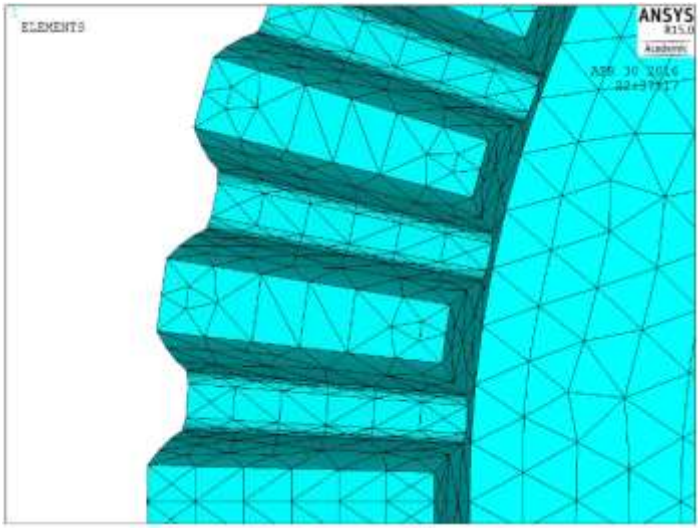

Figure 14: Zoomed in Teeth Mesh

The mesh shown was created with the smallest element size the ANSYS Teaching Advanced license would allow before reaching the nodal limit. The solution to this problem was to utilize sub-modeling on a small section of the gear.

Sub Model Mesh

The section that was modeled was three gear teeth. The three teeth were chosen to eliminate the chance of stress occurring at the boundary of the sub model. The sub model mesh is shown below in Figure 15.

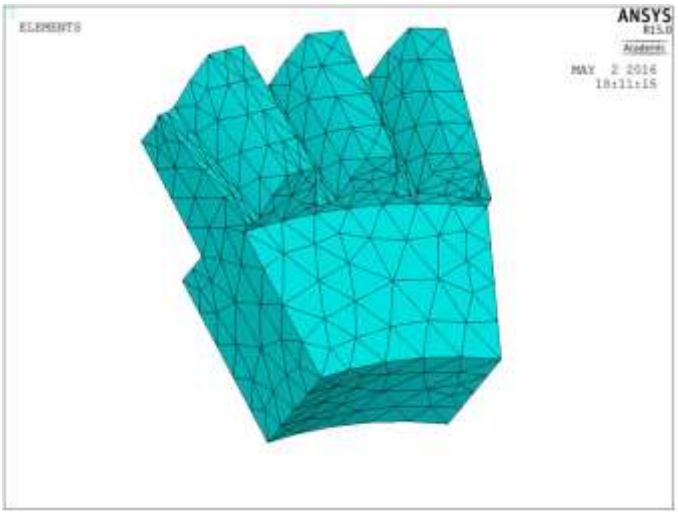

Figure 15: Course Sub Model Mesh Element Size .2 in

With the use of sub modeling a much finer mesh was achieved for the gear teeth. This mesh can be seen below *Figure 16.* The sub model was used to perform a convergence study on the maximum Von-Mises stress.

Figure 16: Refined Sub Model Mesh .05 in Element Size

Static Convergence Study

The mesh size was changed to perform a convergence study on the maximum Von-Mises stress. The mesh size was changed starting at .2 in until a either a converged value was reached or the nodal limit of the program was exceeded. The graph of this study is shown below in Figure 17.

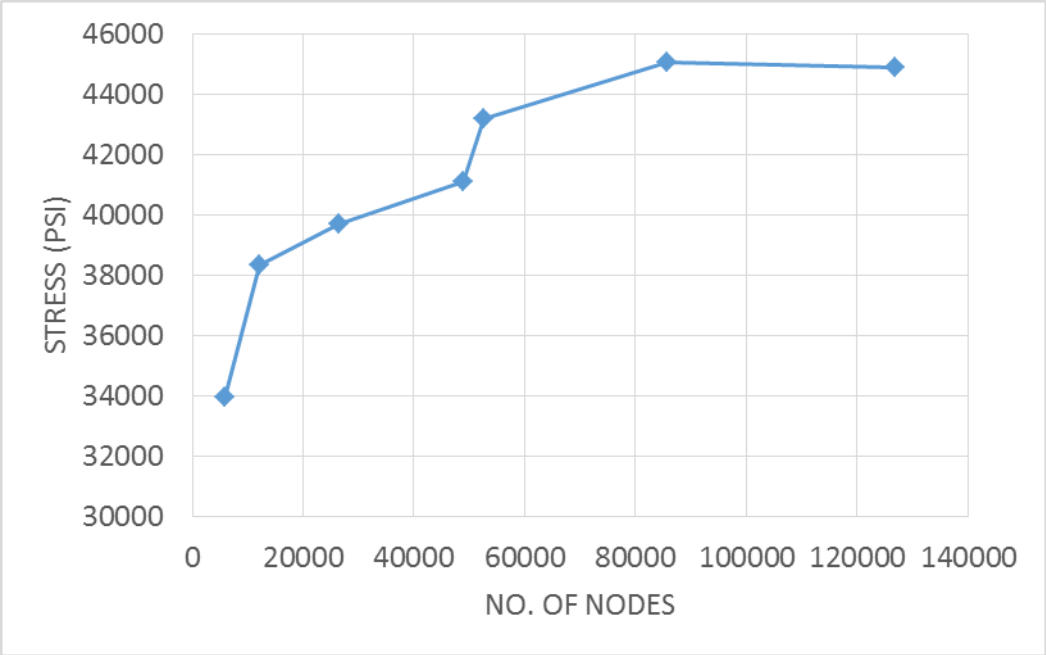

Figure 17: Static Analysis Convergence Study

The stress was found to converge with 90k to 125k nodes to a value of 45,000 psi. The element size and mesh used for the result comparison are shown above in Figure 16.

Static Analysis Results

The deformation in both the global and sub modeled are shown below in Figure 18 and XXXXX respectively.

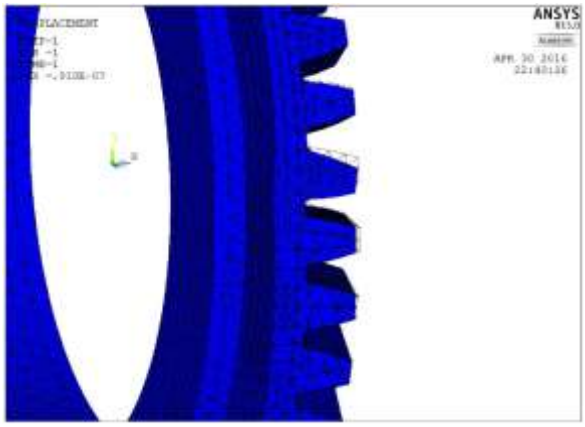

Figure 18: Full Model Deformation

Figure 19: Sub Model Deformation

Both the full and sub model can be seen to deform in the same manor but with different values. This is due to the non-convergence of the course full ring gear model. The deformation can be seen to not only effect the gear tooth that the force is applied to but also the adjacent tooth, this is due to the deformation of the gear flange. This deformation can be seen to be a value of .638E-3 in.

The Von-Mises stress for both the full ring gear model and the sub model are shown below in Figure 20 and Figure 21 respectively.

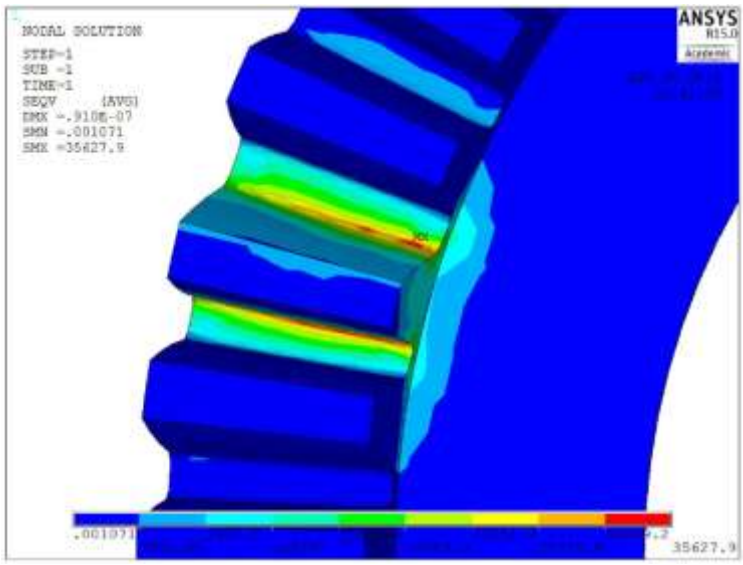

Figure 20: Full Model Von-Mises Stress

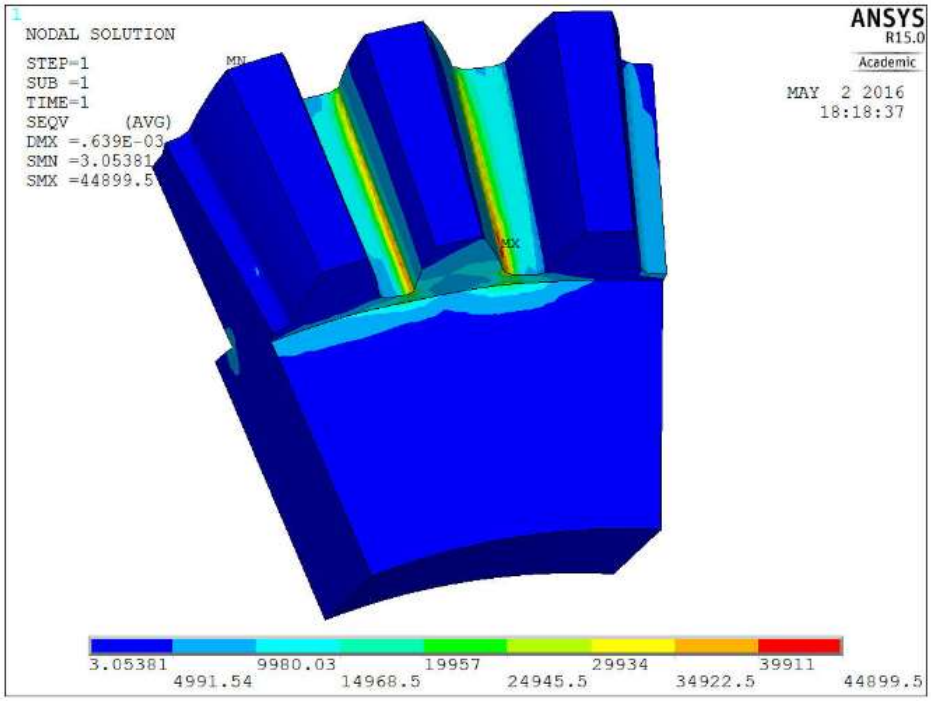

Figure 21: Sub Model Von-Mises Stress

When comparing the full model to the sub model for the Von-Mises stress the contour shape of the stress distribution can be seen to be the same between the two models, also the maximum stress is occurring in the same place at the root of the tooth. The values of the stress are shown too different. The full model has a maximum stress of 35,627 psi while the sub model has a maximum stress of 44,899 psi. The difference in the stress values is due to the global model not being converged. When comparing the stress to that of the analytical value found by Equation 4. There was a 9.2% error. The static analysis

shows that the ring gear is not reaching failure. With the ultimate tensile strength of the gear material being 290,000psi the gears have a static loading safety factor of 6.

Contact Analysis

The contact between the ring and pinion gear was now modeled. The contact analysis will provide insight on which gear is failing and also show if the gears are deforming out of mesh. The boundary conditions, loading and mesh were conducted in ANSYS Work Bench and then imported into APDL for post processing

Contact Analysis Mesh

The mesh for the contact analysis was created using the same elements used for the static analysis, with the addition of contact elements along the gear teeth. The mesh was refined in a similar fashion to that of the static analysis for check for convergence of the maximum Von-Mises stress. The full assembly mesh can be seen below in Figure 22. The contact elements can be seen in Figure 23. The contact elements were chosen to allow for a possible contact between three sets of the gear teeth.

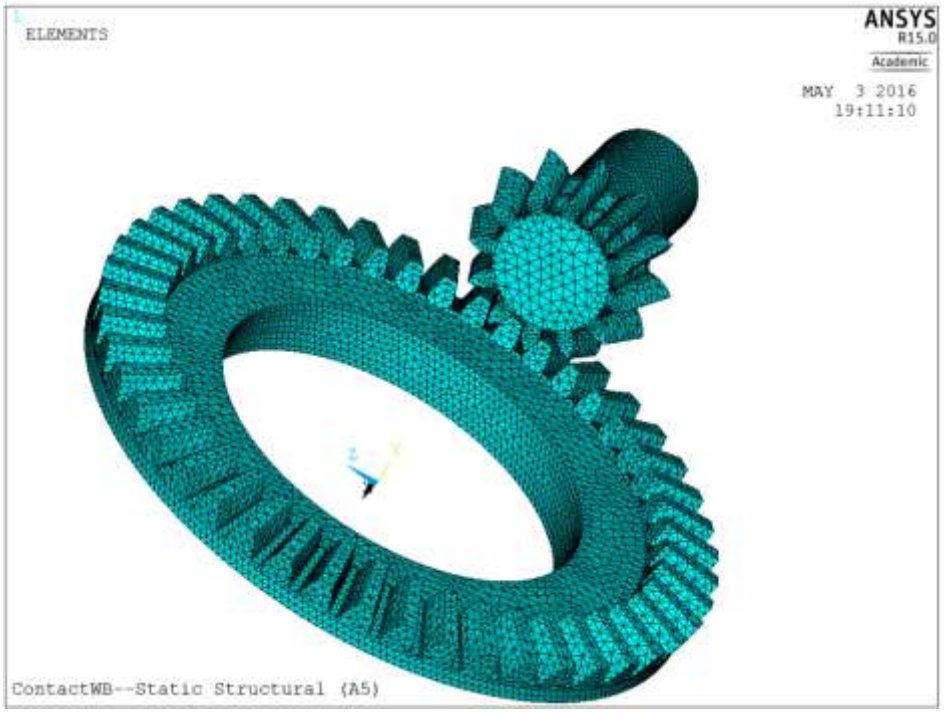

Figure 22: Full Ring and Pinion Mesh Element Size .09 in

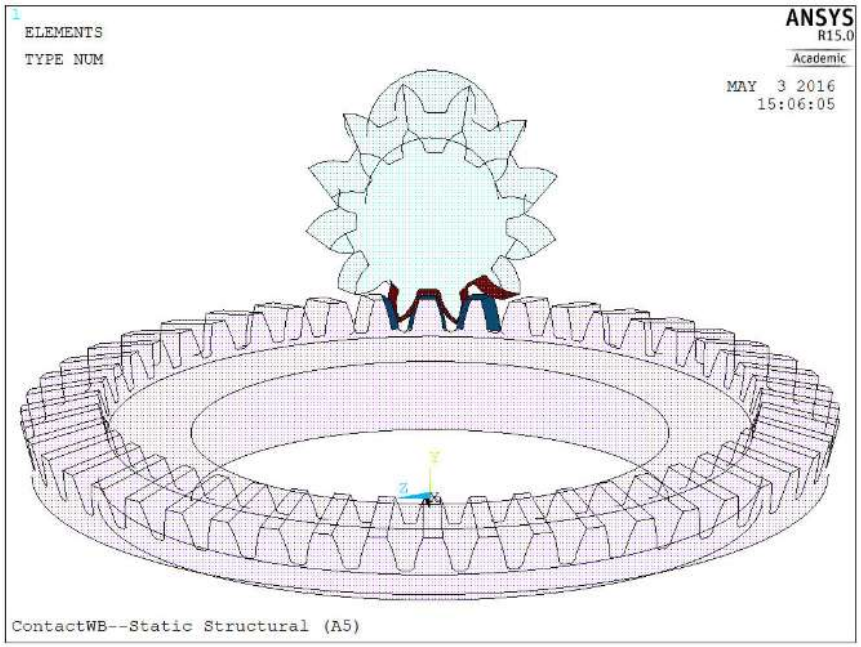

Figure 23: Contact Elements

The contact was setup to be flexible to flexible. With this type of analysis both of the gears are allowed to deform. This allows for the analysis in deflection of both gears. The contact and target surfaces were also defined such the larger gear, ring gear, was set to be the target surface and the pinion gear was set to be the contact surface.

Contact Analysis Boundary Conditions

The boundary conditions for the contact analysis consisted of fixing the ring gear in the same manner as the static analysis while also fixing the pinion gear as well. The calculated pinion shaft torque was applied to the rear surface of the shaft. The Displacement constraints can be seen below in Figure 24. Within this figure the ring gear has all degrees of freedom constrained similar to the static analysis where the pinion gear has been constrained in the x and y along the shaft surface and the front face. The moment is shown by the blue arrow on the rear surface of the pinion shaft.

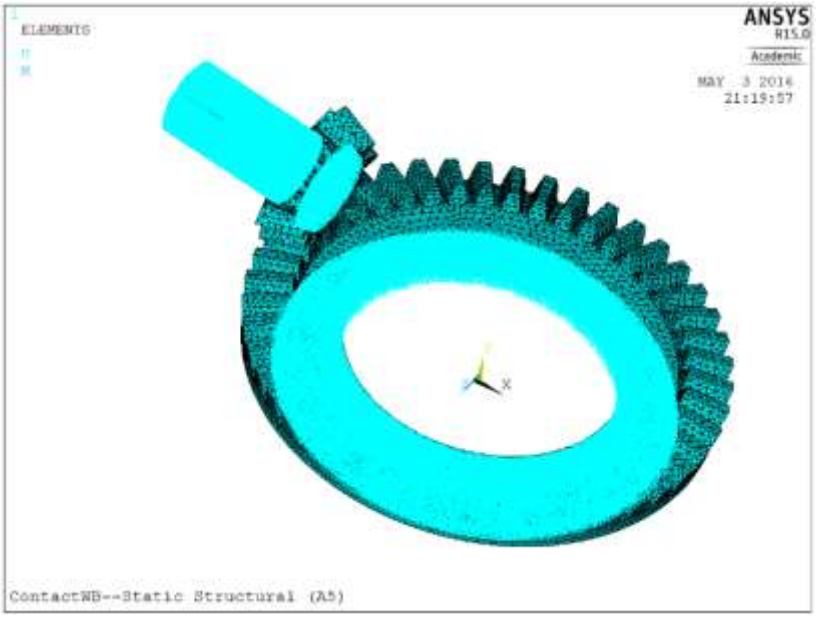

Figure 24: Contact Boundary Conditions

Contact Analysis Convergence Study

The convergence study was conducted on the contact analysis for first the maximum Von-Mises stress. The mesh size was changed from .9 in to .09 in. The stress was found to converge to a value of 266,850 psi. The convergence plot can be seen below in Figure 25.

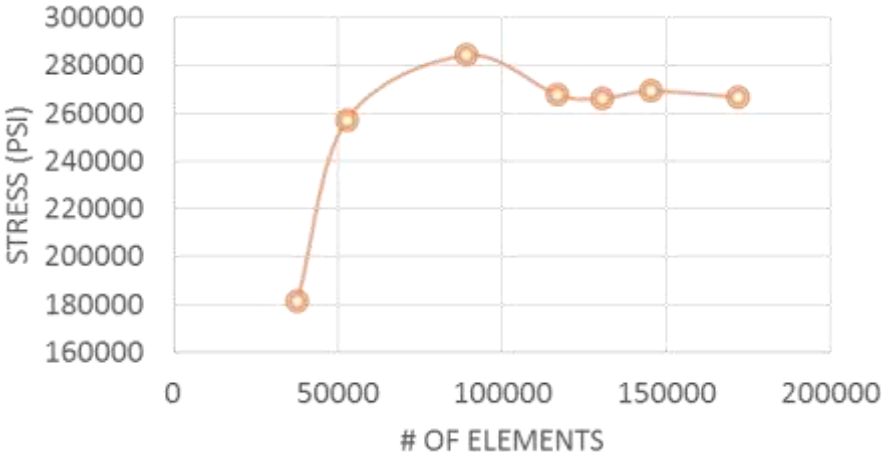

Figure 25: Contact Stress Convergence

A convergence study was also conducted on the contact pressure. The change to mesh was to refine the contact elements size. This was done by refining the mesh on the gear teeth surfaces in mesh. The convergence graph is show below in Figure 26

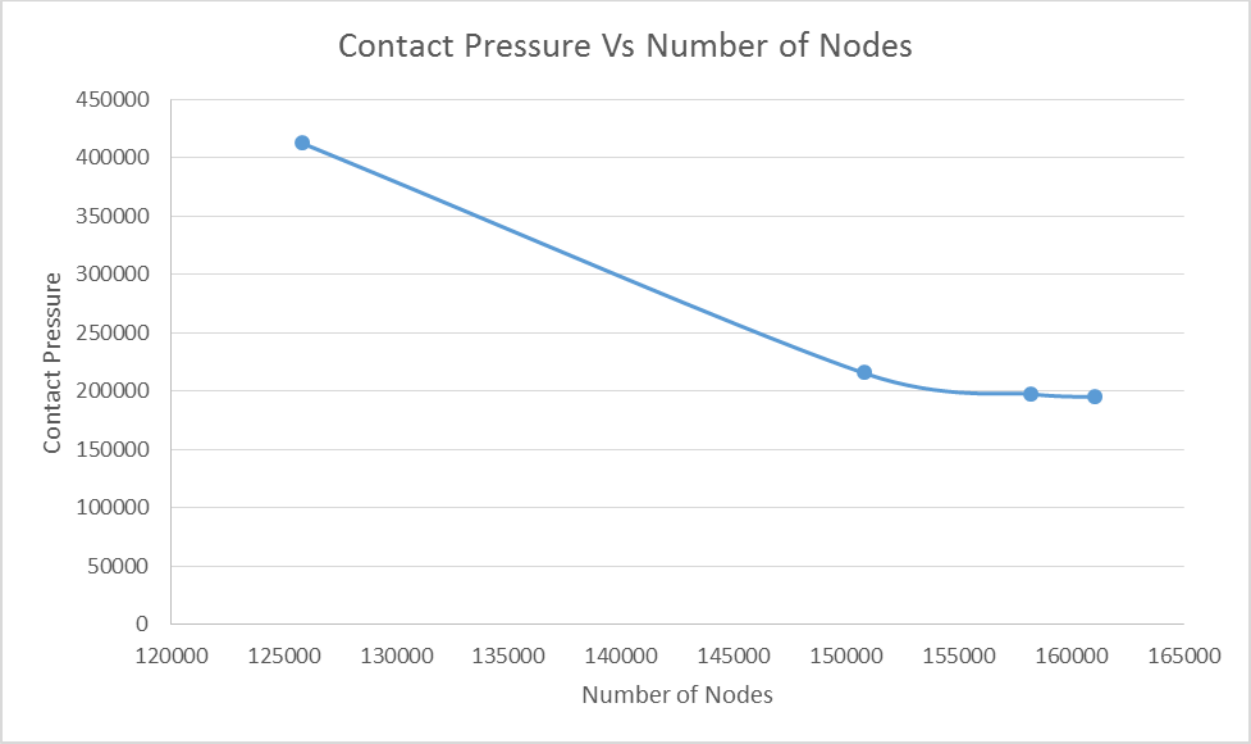

Figure 26: Contact Pressure Convergence

The contact pressure was found to converge with a contact element size of 0.076 in and to a value of 195050 psi.

Contact Analysis Results

The results were taken from the converged mesh which is shown above in Figure 22. The Von-Mises is shown below in Figure 27. It can be seen that the maximum stress occurs at the root of the pinion tooth, while the ring gear is seeing stress with a similar value to the static analysis results.

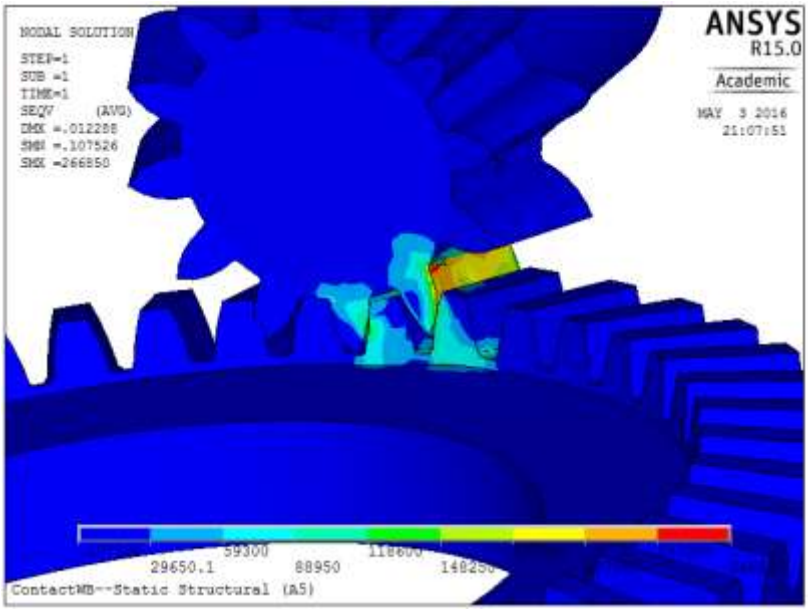

Figure 27: Contact Analysis Von-Mises

The maximum stress is also seen to occur on the tooth that is about to leave mesh. This is expected due to the large bending moment that is applied when the line of action on the gear is reaching the gear end. The maximum stress that was found was 266,850 psi. This stress when compared to the 234,950 psi analytical result shows an 11.97% error. The gear is also operating near the yield strength, with a safety factor of only 1.08, of the hardened steel material.

The contact pressure was also analyzed in along the contact surfaces. The contact pressure plays a direct role in the chipping of the hardened gear teeth surfaces. An image of the actual gear modeled in this simulation is shown in Figure 28. It can be seen that the gear is suffering from pitting/chipping along the rear edge of the tooth surface.

Figure 28: Ring Gear Tooth Chipping

The contour plot of the contact pressure can be seen in Figure 29. The location of the maximum contact pressure is located in the same place that the actual gear is suffering from failure. This seems to indicate that the contact pressure in that location is possibly too high.

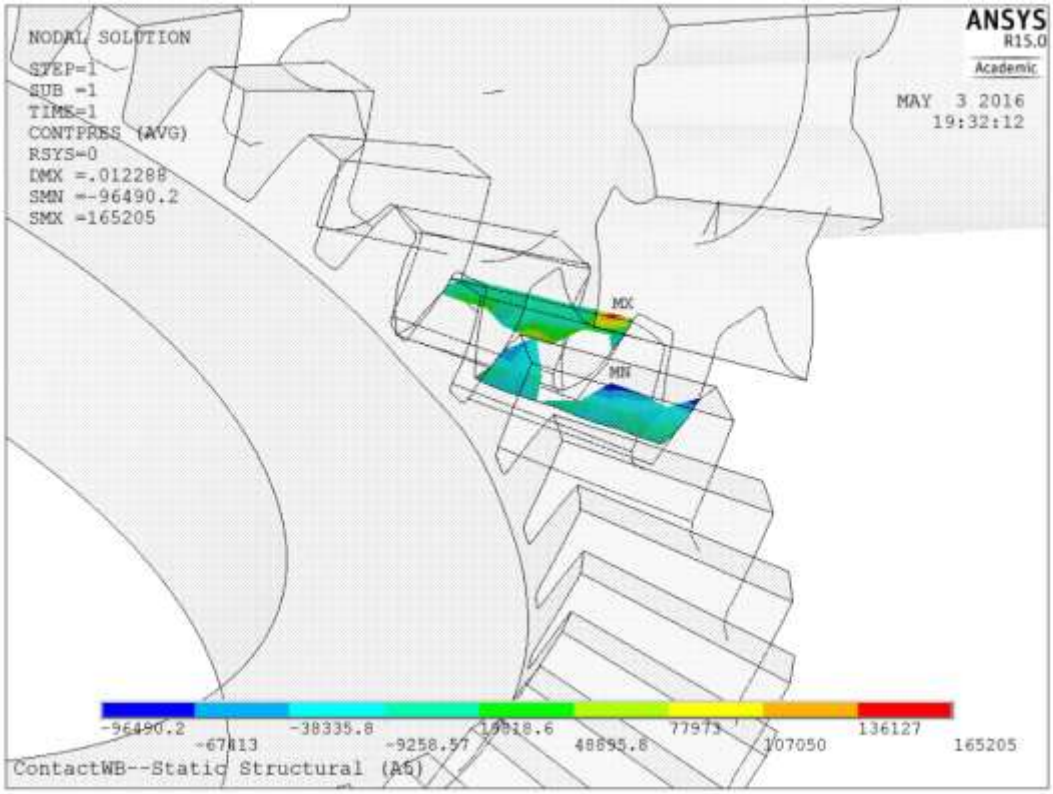

Figure 29: Contact Pressure Plot

Result Conclusion

The ring gear can be seen to be operating below the yield strength of the material, in both the analytical solution and the ANSYS results. The pinion gear is operating close to yield. This indicates that either the ring gear is failing due to loading. The simulation results appear to be an accurate representation of the stresses in the gear train with the small difference from the analytical values. The gears may also be failing due to fatigue and wear. The gears were produced between 40 and 50 years ago, and before they were used in the pulling tractor they were used in a stock cub cadet garden tractor.

Challenges Overcome

The first issue that was encountered was the importation process from SoildWorks to APDL. When the IGES files were created in SoildWorks ANSYS would either import only a surface or there would be tolerance issues. The solution to this problem was to reopen the IGES files in PTC Creo and then resave the IGES as a solid. When the IGES was imported into APDL after this conversion the files would open when using either the smallest tolerance or the tolerance from the file.

Another issue that was encountered was the nodal/element limit the academic teaching advanced license has. With this limit a converging mesh was not possible to be reached with the full ring gear model during the static analysis. The first attempt at a solution was to refine only the area around the tooth that the force was being applied to, this lead to poor transition areas between the elements. This can be seen below in Figure 30.

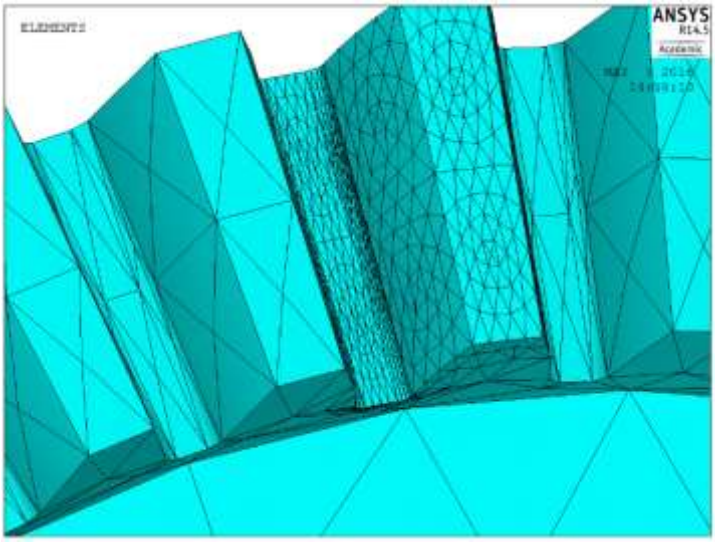

Figure 30: Poor Mesh Transition Areas.

The solution to these issues was to apply sub modeling to the ring gear. The sub modeling allowed for a smaller element size to be used which resulted in a finer mesh. The sub model also removed the poor transitions form meshed area to meshed area. This allowed for the results of the simulation to reach a converged value.

The final issue that was encountered was the application of the boundary conditions for the contact analysis. The conditions were applied with Workbench. The model was then imported back into ANSYS APDL for solution and post processing. This allowed for a contact analysis solution to be reached.

Future Work

The future work that can be done form this project would be to perform fatigue analysis on the gears. The gears are operating close to their failure point but are also showing the effects of figure and wear, as shown by the pitting on the gear faces. The other area that could be expanded on would be to change the type of bevel gear to either a spiral bevel or hypoid bevel to see it the stress is affected. The final extension on this project would be to possibly add in the differential model to the analysis to see the effect on the housing. This would allow for an analysis if the gear deformation would lead to differential failure.

Works Citied

1. "Modifying Cub Cadet Transaxles for Heavy Use And/or Pulling Applications." Modifying Cub Cadet Transaxles for Heavy Use And/or Pulling Applications. Web. 16 Apr. 2016.
2. Budynas, Richard G., J. Keith. Nisbett, and Joseph Edward. Shigley. Shigley's Mechanical Engineering Design. 9th ed. New York: McGraw-Hill, 2011. Print.

APPENDIX

Ring Gear Drawing

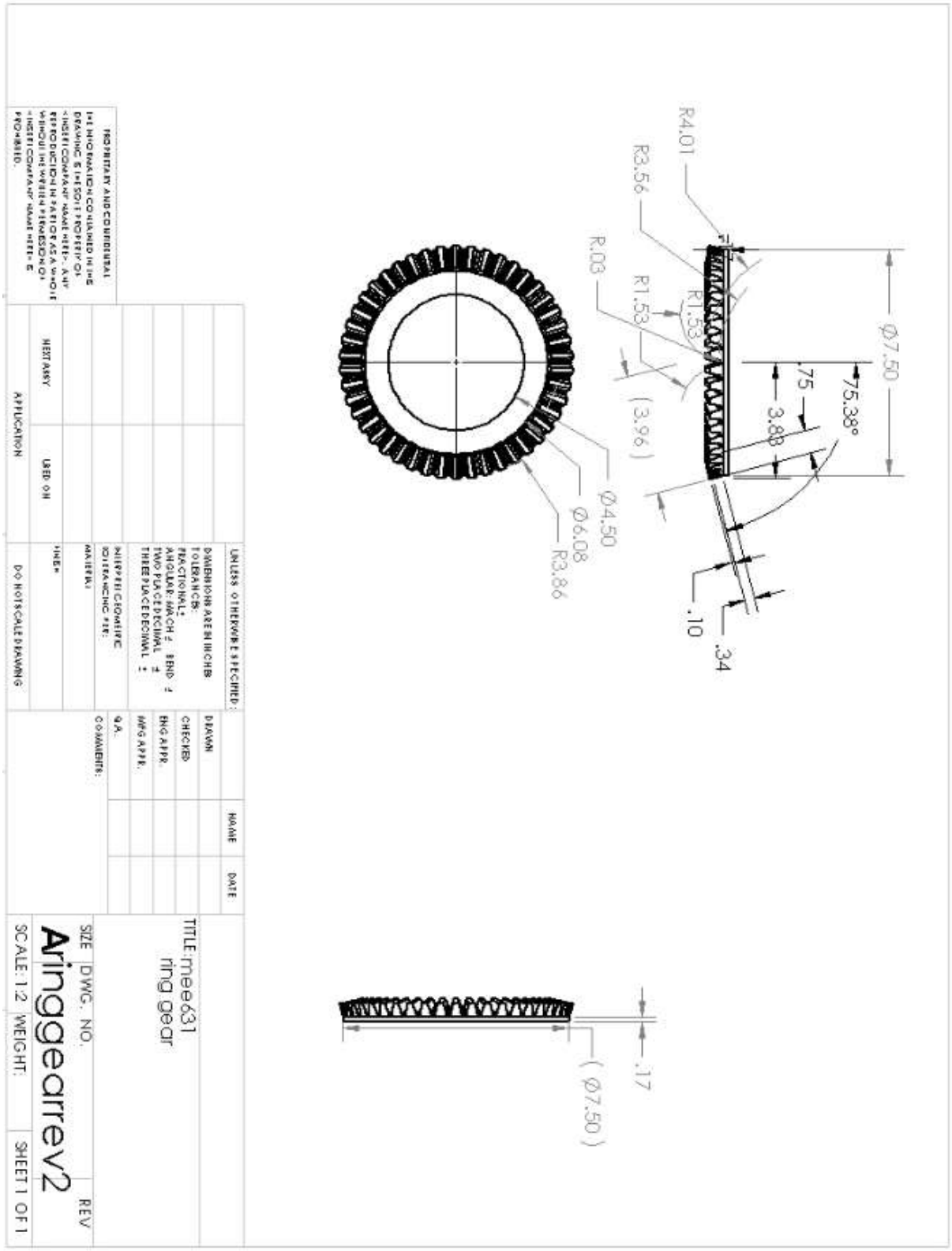

Pinion Gear Drawing

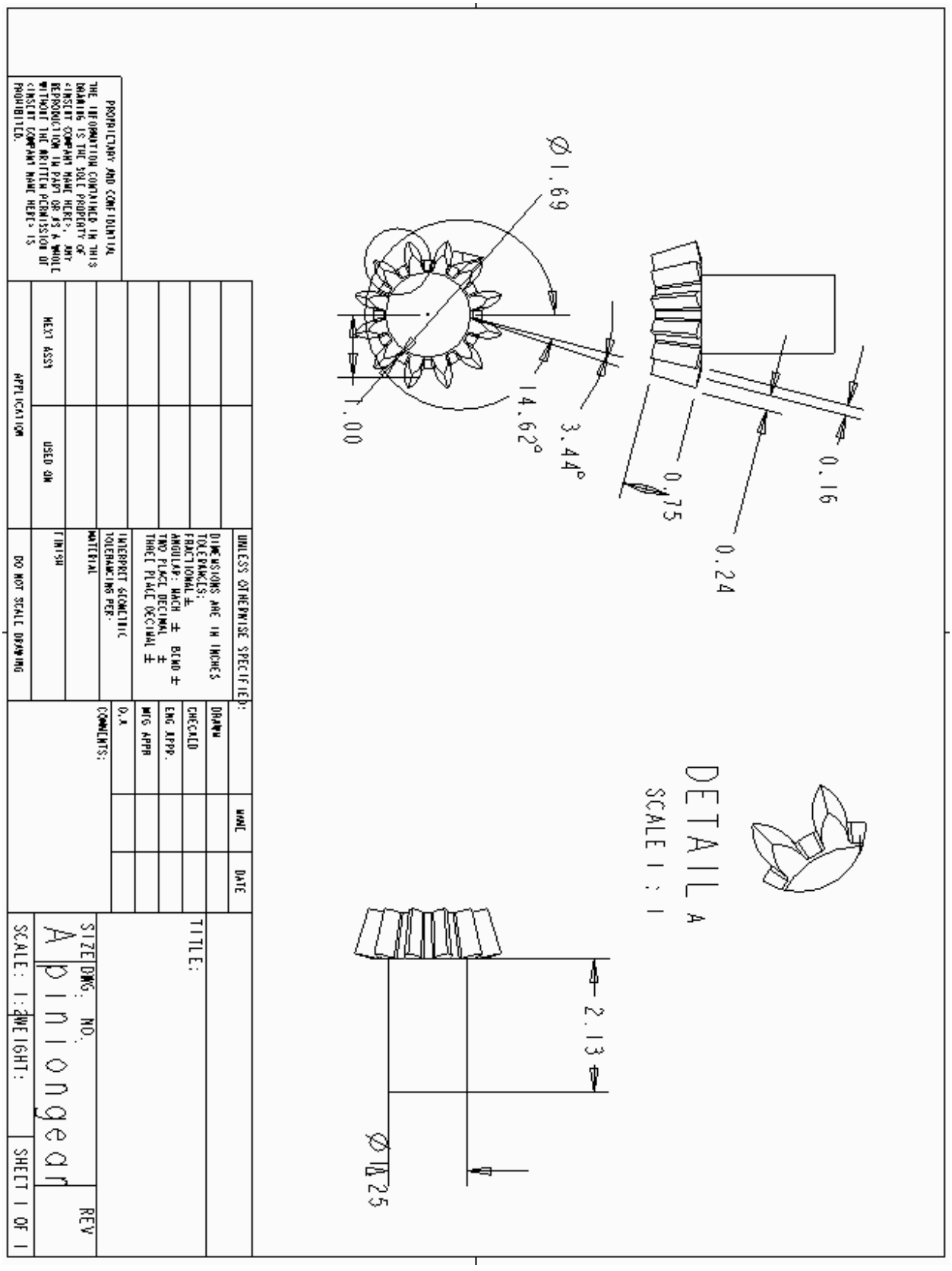

MATLAB FORCE CALCUATION CODE

```
clear all
%engine torque from rpm and horsepower rating in ft lbs
rpm=4000;
hp=30;
enginetorque=(hp*33000)/(2*pi*rpm)
%gear box ratios
%intial reduction
topgear=12;
biggear=84;
ratio=84/12;
%2nd gear
inputgear2=21;
outputgear2=31;
ratio2=31/21;
%3rd gear
inputgear3=23;
outputgear3=29;
ratio3=29/23;
%final ratios
fratio2=ratio*ratio2
fratio3=ratio*ratio3;
%pinion gear shaft torque
shafttorque2=enginetorque*fratio2*.96
shafttorque3=enginetorque*fratio3*.96

%force normal to gear surface
 delta=14.5; %pressure angle
 ravg=.86/12; %in tooth radius average
 W=shafttorque2/(ravg*cosd(delta))
%pitchline Velocity used to determin Kv
npinion=4000/fratio2
V=(pi*npinion*6)/12;
%force normal to gear surface
delta=14.5; %pressure angle
ravg2=4.5/12; %in tooth radius average
 %analytical bending stress on gear teeth AGMA
 pd=6; %diametric pitch.
 F=.75; %face width
 k0=1.25; %overload factor table 15.2 shigleys
 kv=1.4; %dynamic factor figurer 15-5 shigleys
 ks=.4876+.2131/pd%Size factor for bending pg 793 shigleys
 km=1.1+.00036*F^2%Load distribution Factor 15-11
 kx=1;
 J=.165; %Bending Strength Geometry Factor fig 15-7
 Cp=.29; %Elastic Coefficient
 I=.0075;  %Geometry Factor For pitting resistance  fig15-6
 cs=.125*F+.4375 %Size Factor For pitting Resistance 15-9
 cxc=2; %Crowning Factor for Pitting Resistance 15-13 uncrowned teeth.


 Sc=Cp*(W/(F*pd*I)*k0*kv*km*cs*cxc)^1/2 %Fundamental Contact Stress Equation
 St=(W/F)*pd*k0*kv*(ks*km)/(kx*J)%AGMA Dynamic Bending Stress Equation for
bevel gears equation 15-3 shigleys p.791
```

Static Convergence Mesh

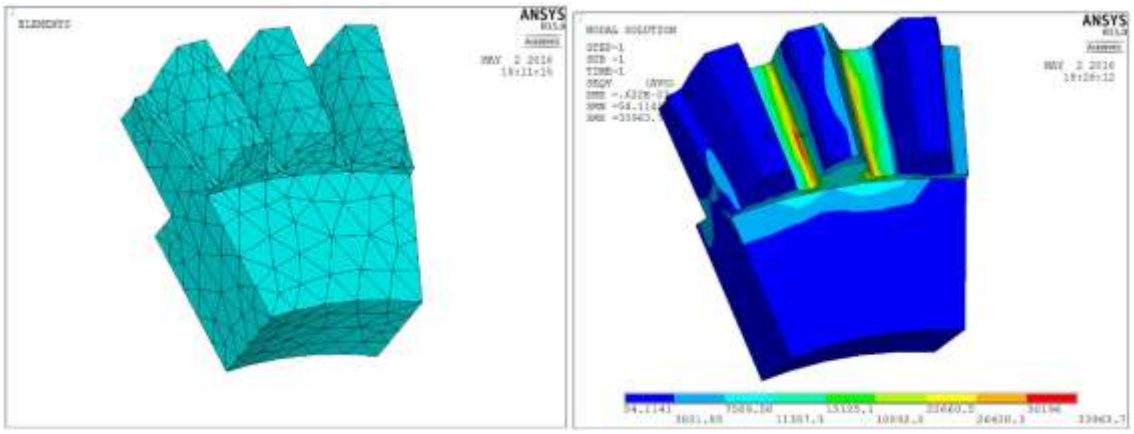

Appendix 1: .2 Mesh and Von-MIses

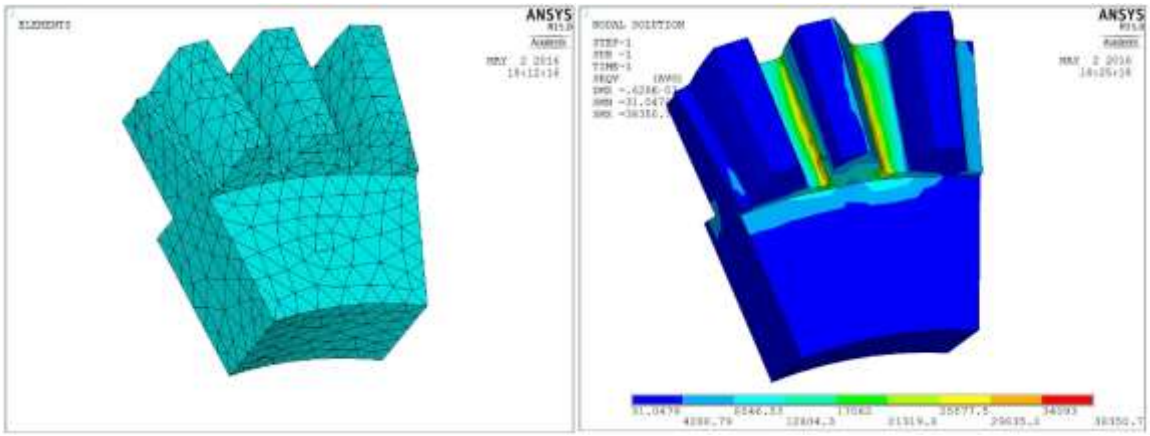

Appendix 2: .15 Mesh and Von-Mises

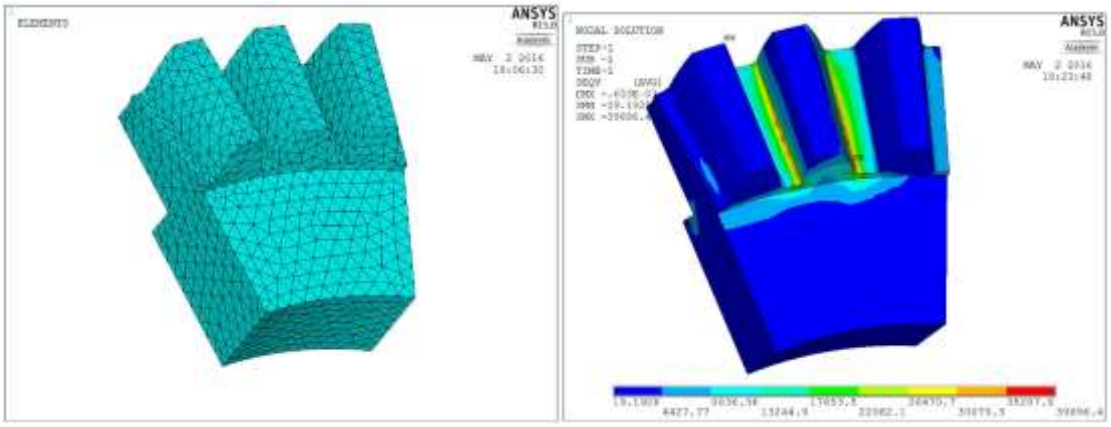

Appendix 3: .1 Mesh and Von-Mises

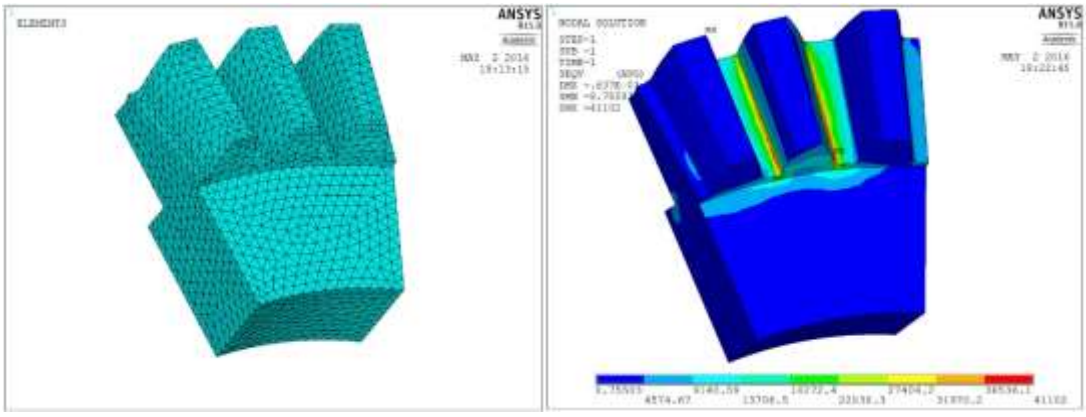

Appendix 4: .075 Mesh and Von-Mises

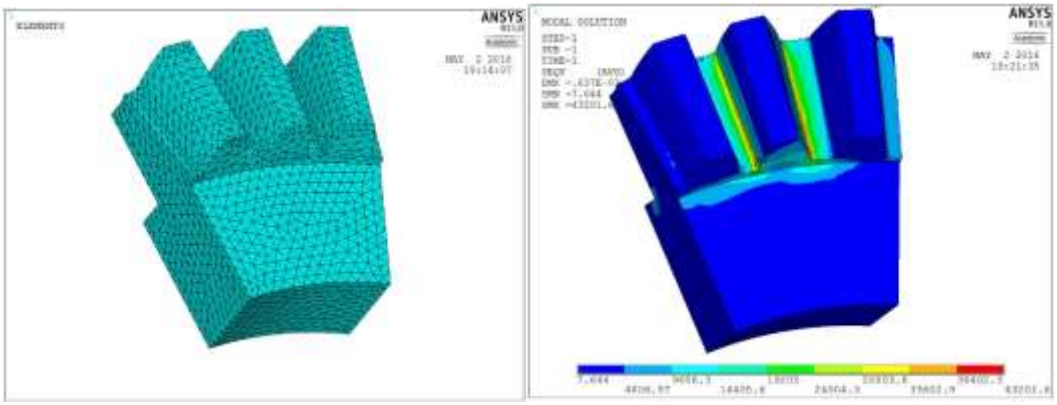

Appendix 5: .072 Mesh and Von-Mises

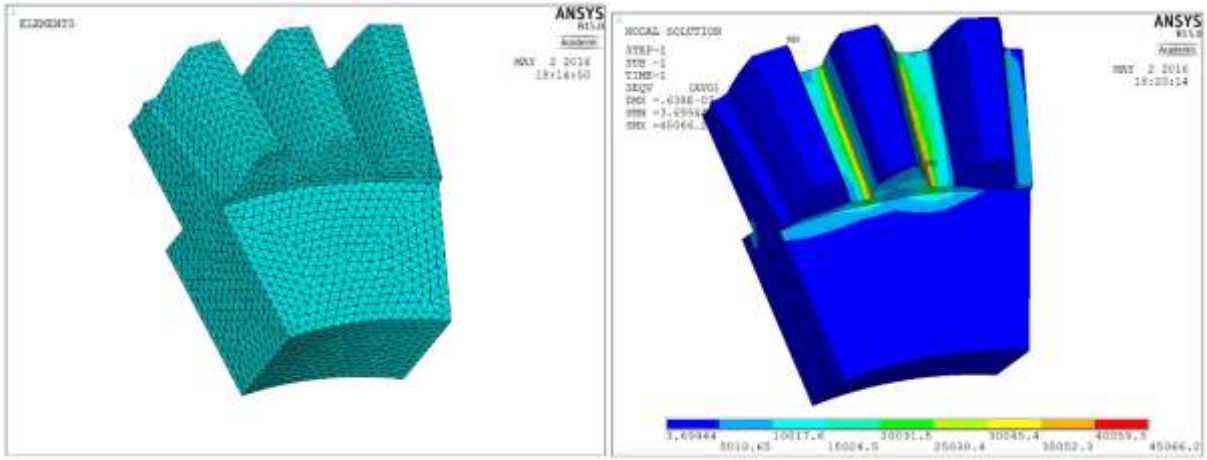

Appendix 6: .06 Mesh and Von-Mises

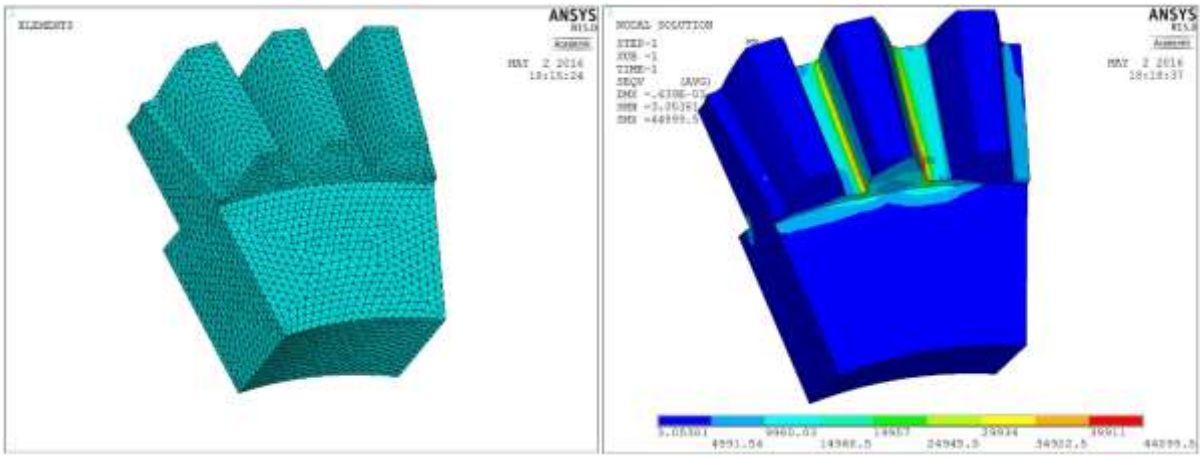

Appendix 7: .05 Mesh and Von-Mises